Compact model and detailed balance limit for a dual n-type direct Z-scheme heterojunction

Johan Lauwaert[1,*] and Nithin Jacob[1]

[1] *Department of Electronics and Information Systems, Ghent University, Technology Park 126, 9052 Zwijnaarde, Belgium*

(Dated: January 23, 2024)

This paper presents a comprehensive study on a compact model and the detailed balance limit for a dual n-type direct Z-scheme heterojunction. The direct Z-scheme catalysis holds immense promise in solar energy conversion due to its simple structure and potential for high efficiency. The compact model developed in this work describes the current-voltage (IV) characteristics of the staggered heterojunction under one-sided illumination.

The model incorporates fundamental principles including charge neutrality, surface recombination, thermionic emission over the barrier, and surface potentials. By considering these factors, the IV curve of the staggered heterojunction is captured, shedding light on the charge transfer and separation processes within the device. The heterojunction device consists of two photosystems: photosystem one (PSI) with a wide band gap, where the oxidation or consumption of electrons from reactants take place and photosystem two (PSII) with a narrow band gap, where the reduction reaction or supply of electrons to the reactants take place.

Furthermore, the paper establishes the detailed balance limit for the efficiency of the dual n-type direct Z-scheme heterojunction. The maximum achievable efficiency, estimated to be 11.4%, is determined by the interplay between the band gap of PSII and the empirical relation for the maximum barrier for electrons leaving PSII. This detailed balance limit represents the highest conversion efficiency that can be attained, accounting for carrier generation, recombination, and charge transfer mechanisms. The compact model and the derived detailed balance limit provide valuable insights for designing and improving the performance of direct Z-scheme heterojunctions, with implications for artificial photosynthesis and renewable energy applications.

I. INTRODUCTION

The development of efficient and sustainable energy conversion technologies has become increasingly crucial in the face of global energy and environmental challenges. Artificial photosynthesis[1], inspired by natural photosynthesis, offers a promising avenue for converting solar energy into chemical fuels or electrical energy.[2] Among the various strategies explored in this field, direct Z-scheme heterojunctions have emerged as a promising approach due to their unique structural simplicity and promising charge transfer properties.[3–5] Direct Z-scheme heterojunctions mimic the electron transfer process found in natural photosynthesis, where charge carriers are transferred between different semiconductor materials to achieve efficient separation and utilization of photogenerated charges. This mechanism holds great potential for enhancing the performance of solar energy conversion devices by minimizing recombination losses and improving overall efficiency. In recent years, the development of photovoltaic-electrolyzer (PV-electrolyzer) systems has gained significant attention as an efficient means for solar fuel production. [6] These systems combine photovoltaic cells with electrochemical cells to directly convert solar energy into chemical fuels such as hydrogen or other value-added products. The use of direct Z-scheme heterojunctions within PV-electrolyzer systems or stand alone has shown promising results, offering enhanced performance, improved energy conversion efficiencies or reduction of production cost. Despite the progress in the field, understanding the fundamental limits and performance characteristics of direct Z-scheme heterojunctions remains crucial for further advancements. [7] By a compact model for the device and investigating the detailed balance limit, which sets an upper limit for the conversion of both electric and chemical energy, researchers can gain insights into the intrinsic capabilities and challenges of these systems. In this paper, we present a comprehensive study on a dual n-type direct Z-scheme heterojunction and explore its compact model and the associated detailed balance limit. We propose a theoretical framework that describes the essential features of the dual n-type heterojunction, incorporating relevant physical parameters and charge carrier dynamics. Through calculation, we analyze the maximum electric power that can be extracted from the system and demonstrate that it is limited to 11.4%. Consequently, this value represents the upper limit for the conversion of chemical energy within the system. Our work contributes to the broader understanding of direct Z-scheme heterojunctions and their potential in solar energy conversion. Furthermore, it sheds light on the intricate balance between electric power extraction and chemical energy conversion, offering valuable insights for the optimization and design of future solar fuel production systems. By pushing the boundaries of energy conversion efficiency, we strive to pave the way towards sustainable and economically viable ar-

* Johan.Lauwaert@UGent.be

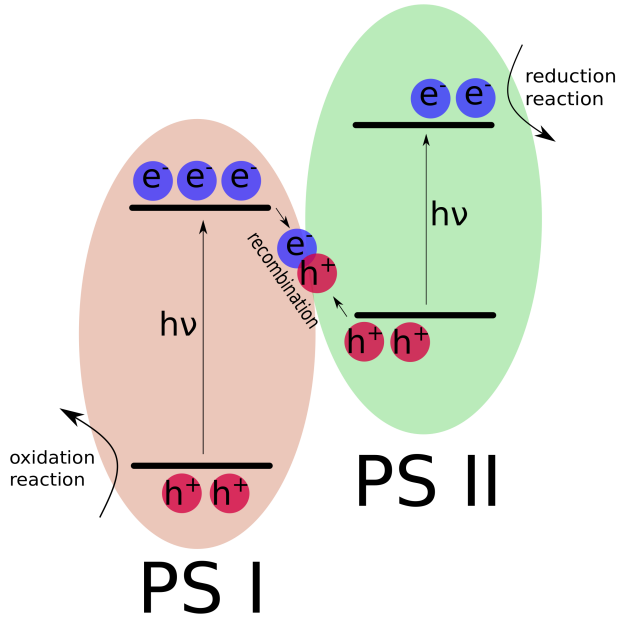

FIG. 1. Diagram showing the direct Z-scheme mechanism

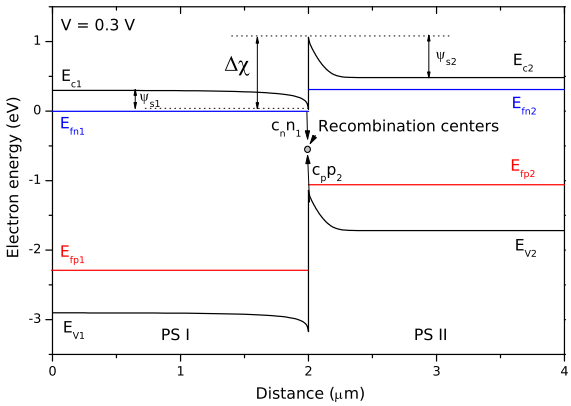

FIG. 2. Band diagram for a direct Z-scheme, the reference for the electron energy is the electron quasi-fermi energy at the contact with PSI

tificial photosynthesis technologies.

II. THE DUAL N-TYPE DIRECT Z-SCHEME BAND DIAGRAM

The dual n-type model for the direct Z-scheme, which serves as the foundation of this research, was initially proposed by Allen J. Bard [9]. Bard's groundbreaking work established the framework for comprehending and harnessing the potential of direct Z-scheme heterojunctions. In this model, two photosystems are identified schematically shown in figure 1: PSI, corresponding to the wide band gap material, and PSII, representing the narrow band gap material. These photosystems play a crucial role in the oxidation and reduction processes occurring within the heterojunction. PSI acts as the oxidation site, where light-induced electron transfer from PSI to an electron acceptor initiates the reduction of the acceptor species. On the other hand, PSII serves as the reduction site, where light absorption promotes electron transfer to PSII, facilitating the oxidation of an electron donor species. Such a model was also implemented in a solar cell simulator by Jacob et al. to explore the impact on the semiconductor properties on the performance of the device [10]. Importantly, it should be noted that while this study focuses on the dual n-type model, a dual p-type model would lead to similar results and findings.

The Z-scheme staggered heterojunction, based on its band diagram shown in figure 2, consists of two distinct photosystems, namely photosystem one (PSI) and photosystem two (PSII), combined within a staggered architecture. The band diagram illustrates the energy levels and band alignments of the materials involved, providing insights into the charge transfer and separation processes.

In this configuration, PSI, typically composed of a wide band gap semiconductor material, is positioned in accumulation, while PSII, composed of a narrow band gap semiconductor, forms an inversion layer. These different charge accumulation states are crucial for achieving efficient charge transfer and separation at the heterojunction interface.

At the interface of PSI and PSII, a staggered alignment is established. This means that the conduction band (CB) of PSII is positioned higher in electron energy compared to the CB of PSI, while the valence band (VB) of PSII is positioned higher in electron energy compared to the VB of PSI. This staggered alignment is intended to facilitate the efficient transfer of photogenerated carriers from PSI to PSII via interface recombination.

In PSI, under illumination, photons with energies higher than the band gap of the material are absorbed, exciting electrons from the VB to the CB. These excited electrons accumulate in the accumulation layer in PSI, creating a high concentration of negative charges. The accumulation layer in PSI is not strongly influenced by the generation of carriers and remains relatively unaffected by the illumination intensity.

In PSII, with its narrower band gap, the material can absorb photons with lower energies, including those in the near-infrared range. When these photons are absorbed, electrons are excited from the VB to the CB, resulting in the generation of electron-hole pairs. However, due to the n-type nature of PSII, the photogenerated holes are quickly trapped and recombine, while the electrons are mobile and form an inversion layer near the interface with PSI. The presence and extent of the inversion layer depend more strongly on the illumination intensity. Higher illumination intensities lead to a more

pronounced and extended inversion layer, while lower intensities result in a weaker inversion layer.

The staggered band alignment at the heterojunction interface enables the transfer of photogenerated electrons from the accumulation layer in PSI to the inversion layer in PSII. This transfer occurs due to the difference in energy levels between the CBs of PSI and PSII. The photogenerated electrons from PSI can migrate to the inversion layer in PSII, where they can participate in further energy utilization processes or be extracted as electrical current.

Understanding the band diagram and the characteristics of the dual n-type Z-scheme heterojunction, including the accumulation layer in PSI and the illumination-dependent inversion layer in PSII, provides valuable insights into the fundamental mechanisms of charge transfer and separation. This knowledge guides the design and optimization of dual n-type Z-scheme heterojunction systems, aiming to maximize energy conversion efficiencies in solar energy conversion technologies.

III. A COMPACT MODEL FOR THE CURRENT-VOLTAGE CHARACTERISTICS

A compact model for a staggered heterojunction can be developed to describe the current-voltage characteristics of the device. This model incorporates key principles such as charge neutrality, surface recombination, and thermionic emission over the barrier. By considering the charge densities, current densities, and surface potentials in each photosystem, the voltage behavior of the heterojunction can be calculated.

The charge neutrality of the device is a fundamental requirement, ensuring that the charge densities per unit area in both photosystem one (PSI) and photosystem two (PSII) are equal. This principle reflects the balance between the accumulation of negative charges in PSI and the inversion layer in PSII. By maintaining charge neutrality, the model can accurately represent the overall charge distribution in the heterojunction.

The space charge per unit area in PSI (Q_1) in accumulation can be written as:

$$Q_1 = \sqrt{2\epsilon_1\epsilon_0 k_B T N_{D1}\left(e^{\beta_1} - 1 - \beta_1\right)} \tag{1}$$

with $\beta_1 = \frac{\Psi_{s1}}{k_B T}$, ϵ_0 is the permittivity of the vacuum, ϵ_1 is the dielectric constant of PSI , k_B is the Boltzmann constant, T is the temperature and Ψ_{s1} is the surface potential induced in PSI by bringing it in contact with PSII. The space charge per unit area in PSII (Q_2) in depletion containing an inversion layer can be written as:

$$Q_2 = \sqrt{2\epsilon_2\epsilon_0 k_B T\left(N_{D2}(\beta_2 + e^{-\beta_2} - 1) + p_{20}(e^{\beta_2} - 1 - \beta_2)\right)} \tag{2}$$

with $\beta_2 = \frac{\Psi_{s2}}{k_B T}$, ϵ_2 is the dielectric constant of PSII, Ψ_{s2} is the surface potential induced in PSII and p_{20} is the minority carrier concentration in the neutral part of PSII. To ensure charge neutrality in the heterojunction the $Q_1 + Q_2 = 0$ condition should be met.

The current density in the staggered heterojunction arises from two primary contributions: surface recombination and thermionic emission over the barrier for electrons in PSII. Surface recombination refers to the process where photogenerated electrons and holes recombine at the heterojunction interface, resulting in current loss. Thermionic emission over the barrier describes the phenomenon where electrons overcome the energy barrier at the heterojunction interface and contribute to the overall current flow. These two mechanisms play significant roles in determining the current density and the efficiency of charge transfer in the heterojunction.

To calculate the voltage behavior of the staggered heterojunction, the surface potentials in both PSI and PSII are considered. The surface potential reflects the energy difference between the Fermi level and the vacuum level at the surface of the material.

The surface potentials induced in both photosystems are connected via:

$$\Psi_{s2} = (E_{c1} - E_{fn1}) - (E_{c2} - E_{fn2}) - \Delta\chi - V - \Psi_{s1} \tag{3}$$

with V the voltage over the structure. In figure 2, which also illustrates Eq. 3, the voltage is chosen $V = 0.3V$. This value, chosen for illustration, is an arbitrary positive value, likely in the vicinity of a potential working point. $\Delta\chi$ is the absolute difference in the electron affinities of the systems and $E_{c1/2} - E_{fn1/2}$ the difference between the majority carrier fermi-level and the conduction band edge in the corresponding photosystem.

Evaluating the current density at the interface enables the calculation of the current-voltage characteristics. At the interface the maximal positive current from PSII to PSI is a recombination current (J_{RJ}) of electrons from PSI with holes from PSII via surface state with a density N_{Ts}.

$$J_{RJ} = \frac{qN_{Ts}c_{n1}n_1c_{p2}p_2}{c_{n1}n_1 + c_{p2}p_2} \tag{4}$$

Herein is n_1 the electron concentration at the PSI side, p_2 the hole concentration at the PSII side, $c_{n1/p1}$ the capture cross-section multiplied by the thermal velocity of these electrons and holes respectively. It can be noted that due to the staggered gap and the prerequisite to have a Z-scheme that the capture rates of electrons from PSI and holes from PSII have the strongest contribution to the Shockley-read-hall recombination current density. In other words, the capture rates for holes from PSI and electrons from PSII and the emission rates can be neglected and as discussed above these mechanisms will reduce the efficiency. Eq. 4 is therefore equal to the hole current from PSII to PSI. Unfortunately, the electrons from PSII, although preferentially contribute to the reduction reaction, they can also enter PSI, lowering the

total current. Luckily, the depletion of PSII at the interface forms a barrier for these electrons. The thermionic emission current density is an underestimate for this electron current and can be written as:

$$J_{Thermionic} = qv_{th}\left(n_1 e^{\frac{-\Delta_X}{k_B T}} - n_2\right) \tag{5}$$

with v_{th} the thermal velocity for electrons and n_2 the electron concentration at the PSII side of the interface. It could be noted that the hole current from PSI to PSII is also lower the efficiency and due to the specific banddiagram will be smaller than the electron current from PSII to PSI. The total current with contains the contribution of the recombination current (Eq. 4) and the thermionic emission current (Eq. 5) is therefore dependent on the carrier concentrations n_1, n_2 and p_2 at the interface. Assuming flat quasi-fermi levels in favor of the maximal recombination current at the interface these concentrations can be written as:

$$n_1 = N_{D1} e^{\beta_1} \tag{6}$$

$$n_2 = N_{D2} e^{-\beta_2} \tag{7}$$

$$p_2 = p_{20} e^{\beta_2} \tag{8}$$

It is remarkable that the hole concentration in PSI (p_1) is absent in these equations describing the available carriers for the chemical reactions, while a hole current at the interaction with electrolyte might match the oxidation reaction better. However, the estimated current at the PSI/ PSII interface forms an upper limit for the available charges. Moreover the electron current in PSI can be converted to a hole current via recombination and generation in the bulk or via preferential selection of carriers in contact with the oxidation reaction.
The maximum power available for the chemical reaction is the maximum of the current density multiplied by the voltage over the structure (i.e. the electrical power). For each illumination condition a certain concentration of holes p_{20} in the neutral part of PS II are created. For each p_{20}, Eq. 3 and the charge neutrality (Eqs. 1 and 2) can be used to calculate the current voltage characteristics.

IV. DETAILED BALANCE LIMIT

The detailed balance limit of the compact model for the staggered heterojunction involves understanding the maximum achievable efficiency of the device. This limit is determined by several factors, including the generation of minority carriers in PSII, the recombination interface between PSI and PSII, and the barrier for electrons leaving PSII.

When photons with energies above the band gap of PSII are absorbed, they generate minority carriers (holes) in PSII. These minority carriers contribute to the overall photocurrent in the device. However, to achieve the detailed balance limit, it is essential to minimize the recombination of these minority carriers before they can contribute to the electrical current. To idealize this situation and to estimate the theoretical limit of artificial photosynthesis via a Z-scheme we assume that the total generated minority carriers in PSII either recombine in the bulk or contribute to the recombination current at the interface with PSI.

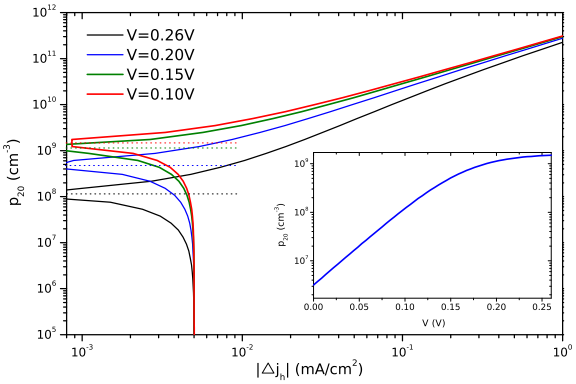

FIG. 3. Graphical representation of the method to calculate p_{20} for different voltages. p_{20} as a function of the hole current density difference $|\Delta j_h|$ (full lines). Determined p_{20} for ideal collection (dotted lines). Inset: determined p_{20} as a function of voltage.

$$J_{RJ} = q\int_0^{t_2} G(x)dx - q\frac{p_{20}t_2}{\tau_2} \tag{9}$$

the point $x = 0$ is for the simplicity chosen at the interface, t_2 is the thickness of PS II and τ_2 the minority carrier life time in PS II. The longest life time of the minority carriers τ_2 is obtained when only radiative recombination is present. For radiative recombination this life time can be written as:

$$\tau_2 = \frac{1}{\beta_{\text{rad}} N_{D2}} \tag{10}$$

with β_{rad} the radiative recombination coefficient . Equation (9) allows to determine the concentration of minority carriers in the neutral part PS II (p_{20}). The graph in Figure 3 visually illustrates the calculation of p_{20}. The horizontal axis represents $|\Delta j_h|$, which signifies the absolute difference between the majority carrier current generated in the material (equation 9) and the collected current through recombination at the interface (equation 4). When this difference in current density reaches zero, indicating complete carrier collection, it defines the ideal scenario for determining p_{20}—shown by the dotted line on the graph. The inset depicts the hole concentration in the neutral part of PSII as a function of voltage, denoted as p_{20}.

The maximum carrier generation rate in PSII corresponds to the photon flux for photons with an energy above the energy gap of PSII (E_{g2}) of the solar spectrum. Both the generation and recombination in the bulk of PSII can be calculated equivalent to the Shockley-Queisser limit for solar cells. Shockley and Queisser provide an in-depth explanation of the detailed equilibrium between generation and radiative recombination in reference [11]. Additionally, reference [12] conducts a comprehensive investigation, encompassing free carrier absorption and auger recombination, specifically tailored for a single-junction Silicon-based solar cell.

The recombination interface between PSI and PSII serves as an ideal current collector for the holes generated in PSII. This means that the holes can efficiently transfer from PSII to PSI maximizing the collection of charge carriers. As a result, the recombination interface plays a crucial role in enhancing the overall performance of the heterojunction.

On the other hand, the barrier for electrons leaving PSII is a limiting factor for the electrical current. While the recombination interface is efficient in collecting holes, the barrier for electrons leaving PSII is never ideal. This non-ideal barrier restricts the flow of electrons, resulting in a limited electrical current and reducing the overall efficiency of the device. Based on the theory of Bethe [13] this current density can be written as:

$$J_{Thermionic} = A^* T^2 \exp\left(-\frac{q\phi_{bn}}{k_B T}\right)\left(\exp\left(\frac{qV}{k_B T}\right) - 1\right) \tag{11}$$

with $A^* = 1.2 \times 10^5 \frac{mA}{cm^2 K}$ the Richardson constant and ϕ_{bn} the barrier height. To estimate the maximum efficiency, the empirical relation of Mead and Spitzer[14] can be utilized, connecting the band gap of PSII with the maximum barrier that can be achieved for electrons leaving PSII.

$$\phi_{bn} = \frac{2}{3} E_g \tag{12}$$

This relationship has been ascribed to the fact that a high peak density of surface states is present at the semiconductor. Surface states that in a Z-scheme need to be present to maximize the recombination current to extract the carriers from PSII. We therefore propose that this relationship defines a realistic maximum for this barrier preventing electrons to contribute to the reduction reaction.

In this approach, we first examine how minority carriers, specifically holes within PSII generate and recombine. An important aspect of our model is the ideal recombination interface, which efficiently gathers all the holes. This allows to calculate the minority carrier concentration in the neutral part p_{20} as discussed above. However, the presence of a non-ideal electron barrier creates a current loss by allowing some electron current, ultimately reducing the overall efficiency. This limit critically defines the efficiency boundaries of the compact model for the staggered heterojunction, particularly as both the hole and electron currents are voltage-dependent. These currents collectively form the total current-voltage (IV) characteristics of the system. This limit represents the maximum achievable efficiency of the device, considering the fundamental constraints of the band gap of PSII. Figure 4 shows the efficiency as a function of E_{g2}, demonstrating a peak efficiency of 11.4% when the PSI band gap exceeds 4.0 eV. Our model integrates the PSI band gap by simulating the parasitic absorption of photons above this threshold. The optical generation of carriers in PSI prompts a Fermi level split, notably enhancing carrier concentration p_1 at the interface. This increased hole concentration diminishes efficiency by emittion of holes over the hole barrier, akin to the electron barrier in PSII. Consequently, our depiction of maximum achievable efficiency solely considers the results of parasitic absorption.

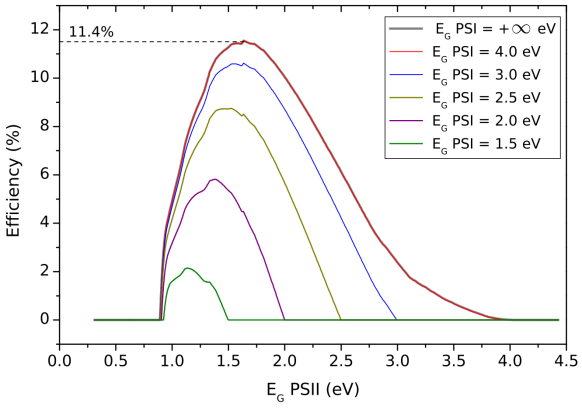

FIG. 4. Maximal efficiency as a function of the band gap energy of PSII for different band gap energies of PSI. The curves for $E_{g1} = 4.0$eV and $E_{g1} = +\infty$eV match exactly.

V. CONCLUSION

In conclusion, this paper presented a comprehensive analysis of a compact model for the current-voltage (IV) curve of a staggered heterojunction in the context of a direct Z-scheme. The model incorporated key principles such as charge neutrality, surface recombination, thermionic emission over the barrier, and surface potentials to accurately describe the behavior of the heterojunction under illumination from one side.

By considering the unique characteristics of the staggered heterojunction, including the accumulation layer in photosystem one (PSI) and the illumination-dependent inversion layer in photosystem two (PSII), the compact model provided valuable insights into the charge transfer

and separation mechanisms within the device.

Furthermore, the paper established a detailed balance limit for the efficiency of the staggered heterojunction. This limit was estimated to be 11.4%, based on the empirical relation between the band gap of PSII and the maximum barrier for electrons leaving PSII. This efficiency limit represented the maximum achievable conversion efficiency for the device, taking into account factors such as carrier generation, recombination, and charge transfer processes.

The compact model and the derived detailed balance limit offer a solid foundation for understanding and optimizing the performance of staggered heterojunctions in solar energy conversion applications. By accurately characterizing the IV curve and identifying the efficiency limit, this research provides important guidelines for enhancing the design and operation of direct Z-scheme heterojunctions.

Future studies can build upon this work by exploring strategies to minimize recombination losses, optimize material parameters, and improve charge transfer kinetics within the staggered heterojunction. Additionally, investigating alternative device architectures may further push the efficiency limit and enable even higher performance in direct Z-scheme heterojunctions.

Overall, this research contributes to the broader field of artificial photosynthesis and solar energy conversion by providing a compact model that captures the essential aspects of a staggered heterojunction and by establishing a detailed balance limit for its efficiency. These findings pave the way for the development of more efficient and sustainable energy conversion technologies based on direct Z-scheme heterojunctions.

ACKNOWLEDGMENTS

The authors would like to acknowledge Catalisti VLAIO (Vlaanderen Agentschap Innoveren & Ondernemen) for their funding through the Moonshot SYN-CAT project (HBC.2020.2614).

[1] Smith, A. B., Johnson, M. B., and Walker, A. B. Artificial Photosynthesis: Strategies, Challenges, and Opportunities. ACS Energy Letters, 4(4), 847-855 (2019).

[2] A. Galushchinskiy, R. González-Gómez, K. McCarthy, P. Farràs and A. Savateev, Progress in Development of Photocatalytic Processes for Synthesis of Fuels and Organic Compounds under Outdoor Solar Light, Energy Fuels 36 (9), 4625 (2022).

[3] K. Hojo, S. Nishioka, Y. Miseki, Y. Kamakura, T. Oshima, K. Sayama, T.E. Mallouk, and K. Maeda, An Improved Z-Scheme for Overall Water Splitting Using Dye-Sensitized Calcium Niobate Nanosheets Synthesized by a Flux Method. ACS Appl. Energy Mater. 4 (9), 10145–10152 (2021).

[4] Q. Xu, L. Zhang, J. Yu, S. Wageh, A.A. Al-Ghamdi and M. Jaroniec, Direct Z-scheme photocatalysts: Principles, synthesis, and applications, Materials Today 12 (10), 1042 (2018).

[5] Rehman, Z.U.; Bilal, M.; Hou, J.; Butt, F.K.; Ahmad, J.; Ali, S.; Hussain, A. Photocatalytic CO2 Reduction Using TiO2 -Based Photocatalysts and TiO2 Z-Scheme Heterojunction Composites: A Review. Molecules 2022, 27, 2069.

[6] Jia, J., Seitz, L., Benck, J. et al. Solar water splitting by photovoltaic-electrolysis with a solar-to-hydrogen efficiency over 30%. Nat Commun 7, 13237 (2016). https://doi.org/10.1038/ncomms13237

[7] Linxi Wang, Chuanbiao Bie and Jiaguo Yu, Challenges of Z-scheme photocatalytic mechanisms, Trends in Chemistry, Volume 4, Issue 11, 2022, Pages 973-983, ISSN 2589-5974, https://doi.org/10.1016/j.trechm.2022.08.008.

[8] M.R. Singh, E.L. Clark and A.T. Bell, Thermodynamic and achievable efficiencies for solar-driven electrochemical reduction of carbon dioxide to transportation fuels, PNAS E6111-E6118 (2015).

[9] A.J. Bard, Photoelectrochemistry and heterogeneous photo-catalysis at semiconductors, J. Photochem. 10, 59 (1979).

[10] N.T. Jacob, J. Lauwaert, B. Vermang and J. Lauwaert, Numerical device modeling for direct Z-scheme junctions using a solar cell simulator, Solar Energy 259, 320-327 (2023).

[11] W. Shockley and H.J. Queisser, Detailed Balance Limit of Efficiency of p-n Junction Solar Cells, J. Appl. Phys. 32, 510 (1961).

[12] T. Tiedje, E. Yablonovitch, G. D. Cody and B. G. Brooks, Limiting efficiency of silicon solar cells, in IEEE Transactions on Electron Devices, vol. 31, no. 5, pp. 711-716, May 1984, doi: 10.1109/T-ED.1984.21594.

[13] S.M. Sze and K.K. Ng, Physics of Semiconductor Devices, John Wiley & Sons (2006).

[14] C.A Mead and W.G. Spitzer, Fermi Level Position at Semiconductor Surfaces, Phys. Rev. Lett. 10 (11), 471 (1963).

[15] Hisatomi, T., Kubota, J., and Domen, K. Recent advances in semiconductors for photocatalytic and photoelectrochemical water splitting. Chemical Society Reviews, 43(22), 7520-7535 (2014).